FFI-rapport 2013/02420

Development of LES inflow conditions for turbulent boundary layers

Emma M. M. Wingstedt, Magnus Vartdal,
Andreas N. Osnes and Murat Tutkun

FFI Forsvarets forskningsinstitutt

FFI-rapport 2013/02420

Development of LES inflow conditions for turbulent boundary layers

Emma M. M. Wingstedt, Magnus Vartdal, Andreas N. Osnes and Murat Tutkun

Norwegian Defence Research Establishment (FFI)

31 October 2013

FFI-rapport 2013/02420

1256

P: ISBN 978-82-464-2316-6
E: ISBN 978-82-464-2317-3

Keywords

CFD simulering

Grensebetingelser

Turbulente grensesjikt

Approved by

Monica Endregard	Project manager
Jan Ivar Botnan	Director

English summary

Computational Fluid Dynamics (CFD) is currently the only known physically based method to model dispersion and transport of aerosols and gases in complex urban environments. One of the main challenges with CFD simulations is to prescribe inflow conditions that are varying in time and are compatible to a solution of the Navier-Stokes equations. The primary motivation of this study is to develop and verify a method that provides realistic three-dimensional and time varying velocity fields to be used as inflow conditions for CFD based dispersion and transport modeling.

If unrealistic inflow conditions are used, very large computational domains are usually necessary to ensure realistic wind fields in the area of interest. This increases the computational cost (time and hardware requirements) that may limit the applicability of CFD simulations.

In this study a new method to create inflow conditions was examined by utilizing an experimental database. The method is based on the measured velocity data which are converted to data usable in CFD simulations by using a procedure called linear stochastic estimation (LSE).

The results are promising and it is demonstrated that the method can generate a realistic turbulent boundary layer at a distance only ~ 3 boundary layer thicknesses downstream the inflow plane. Other methods usually require $3-4$ times longer distances. In the atmospheric scale that means the distance is reduced from approximately $3000\mathrm{m}$ to $900\mathrm{m}$, hence the computational domain can be reduced accordingly.

From a scientific point of view, the importance of large scale turbulence on the inflow condition is of interest. This was examined by using proper orthogonal decomposition (POD). The velocity field was reconstructed using different amount of energy and the result indicated a longer transitional region when less energy was used. Further downstream, the predicted turbulence kinetic energy reached the same values.

Sammendrag

Computational Fluid Dynamics (CFD) er på det nåværende tidspunkt den eneste fysisk baserte metoden for å modellere spredning og transport av aerosoler og gasser i komplekse urbane miljøer. En av hovedutfordringene med CFD simuleringer er å bestemme innstrømsbetingelser som varierer i tid og er kompatible med en løsning av Navier-Stokes ligninger. Hovedformålet med denne studien er å utvikle og verifisere en metode som gir realistiske tre-dimensjonale og tidsvarierende hastighetsfelt for bruk som innstrømsbetingelser i CFD beregninger av spredning og transportmodellering.

Ved bruk av uegnede innstrømsbetingelser kreves ofte store beregningsdomener for å oppnå realistiske vindfelt i de interessante områdene. Dette resulterer i økte beregningskostnader som kan begrense bruksområdet til CFD simuleringer.

I denne studien utforskes en ny metode for å generere innstrømsbetingelser ved hjelp av en eksperimentell database. Metoden er basert på målte hastigheter som blir konvertert til et format som kan brukes i CFD simuleringer gjennom en prosedyre som kalles linear stochastic estimation (LSE).

Resultatene ser lovende ut og det blir vist at metoden kan generere et realistisk turbulent grensesjikt bare ~ 3 grensesjiktstykkelser nedstrøms for innstrømningsplanet. Andre metoder krever typisk $3-4$ ganger denne distansen. Ved atmosfærisk skala innebærer dette en reduksjon fra ca. $3000\mathrm{m}$ til $900\mathrm{m}$. Dermed kan beregningsområdet reduseres tilsvarende.

Fra et vitenskapelig synspunkt er effekten av storskala turbulens på innstrømsbetingelsen av interesse. I denne studien ble dette undersøkt ved bruk av proper orthogonal decomposition (POD). Hastighetsfeltet ble rekonstruert med forskjellige energinivåer og resultatene viser at redusert energi resulterer i et lengre transisjonsområde. Lengre nedstrøms sammenfaller den beregnede turbulente kinetiske energien.

Contents

1 Introduction

Computational Fluid Dynamics has become a popular and very promising tool for simulating a variety of flows since the method is directly based on the fundamental physical law known as Navier-Stokes equations, it is generally applicable to a wide range of situations. However, there are still challenges involved. One of the main challenges, especially when it comes to simulating spatially developing turbulent boundary layers, is to correctly prescribe the inflow boundary condition. Due to the sensitivity of turbulence on the initial conditions, unphysical inflow conditions or inflow conditions which lack the dynamics of a turbulence cascade result in very long development distances if, at all, the developed turbulence can be achieved.

There exists several techniques for generating turbulent inflow conditions (for reviews, see Lund et al. (1998), Moin and Mahesh (1998) and Keating et al. (2004)). The most straightforward approach is to simulate instantaneous inflow boundary condition by imposing random fluctuation on the mean velocity profile and then allow natural transition of turbulence to occur. Such an implementation usually gives good results but is often very expensive because natural transition appears far downstream from the inlet, thus requiring larger computational domains. The reason for this is that by imposing random fluctuations, it is not given that these fluctuations are compatible to the solution of Navier-Stokes equations.

The purpose of this work is to investigate a new method to create inlet conditions which will contain as much dynamics as possible in order to shorten the development distance. The plan is to update the inflow plane of a numerical simulation at each time step using the three components of turbulent fluctuations taken from experiment. By using experimental data it is ensured that the turbulent fluctuations are not random but actually consistent with a solution to the Navier-Stokes equations. The experimental database utilized consists of data obtained by synchronized particle image velocimetry (PIV) and hot-wire anemometry (HWA) measurements.

When conducting Large Eddy Simulation (LES) of a developing flat plate boundary it is necessary to use very small time steps. In order to create inflow data with such high temporal resolution, linear stochastic estimation is used. The LSE method uses the conditional information about the flow in order to estimate information in points in space where the flow was not measured. In this manner the experimental data can be converted to data suitable for CFD. By using LSE, the strengths of both measurement techniques is enabled; the very fine spatial resolution provided by the PIV system is used and the missing information, which is the temporal resolution, is obtained by the hot-wire anemometry. Correlations between hot-wire data and PIV data are built and these correlations are used to feed the PIV data with its missing component, i.e., the temporal development.

From a scientific point of view, it is desired to investigate how much of the large scale dynamics really is necessary to include in the inflow field in order to obtain satisfactory numerical results. For that reason, another method known as proper orthogonal decomposition, which decomposes

the flow into its energetic modes according to energy content, is used. The experimental velocity field is reconstructed using different number of modes, corresponding to different amounts of energy.

This report describes the experiment, the theory behind LSE and POD, and a selection of numerical results are shown.

2 Experimental data

The experimental database was created in the large LML (Laboratoire de Mécanique de Lille, France) wind tunnel at a high Reynolds number. The freestream velocity of the tunnel was $10\mathrm{m/s}$ and Reynolds number based on momentum thickness was 19100. The wind tunnel provides a turbulent boundary layer with a thickness of $\delta \approx 30\mathrm{cm}$, which was measured by using a synchronized system of stereo PIVs (c.f. Figure 2.1) and a hot-wire rake consisting of 143 single wire probes (c.f. Figure 2.2). This made it possible to obtain both spatial and time history of the turbulent velocity field.

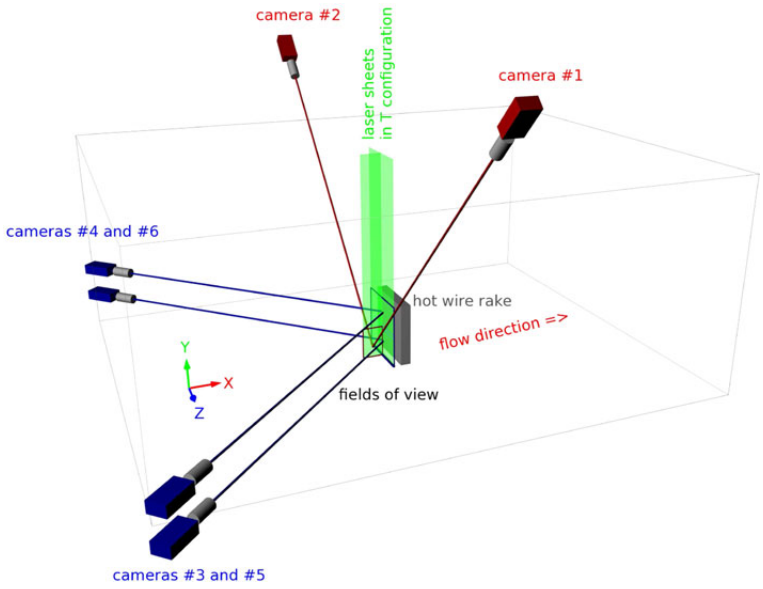

Figure 2.1 Global view of the experimental set up (Coudert et al., 2011).

The PIV measured all velocity components in a $\delta \times \delta$ plane perpendicular to the flow direction with a spatial resolution of $2\mathrm{mm}$, corresponding to approximately 40 wall units. Figure 2.3 shows the contour of the instantaneous streamwise velocity component in the PIV-planes measured for one instance in time.

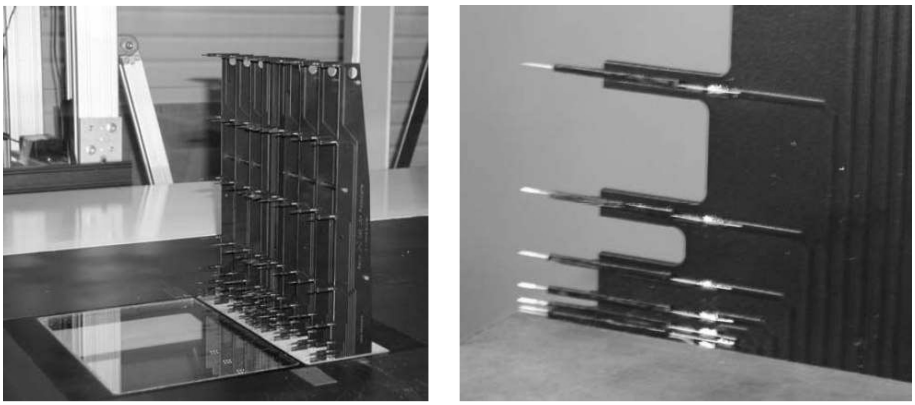

Figure 2.2 Hot-wire rake in place in the LML wind tunnel (left) and zoom on the closest to the wall probes of one individual comb of the rake (right), (Tutkun et al., 2009).

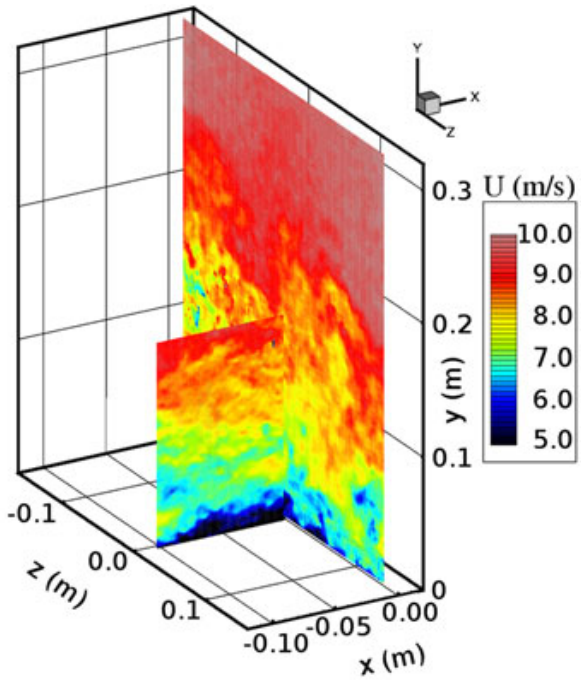

Figure 2.3 Contour of instantaneous streamwise velocity component at $10\mathrm{m/s}$ *(Coudert et al., 2011).*

The hot-wire rake was placed $1\mathrm{cm}$ behind the measured PIV plane and covered an area of approximately $\delta \times \delta$. The hot-wire probes were distributed on an array in a plane normal to the flow, hence only the streamwise component of the velocity was measured. The sampling rate of the hot-wires was $3000\mathrm{kHz}$ and for the PIV $4\mathrm{Hz}$. Hence, the data received from hot-wires had a high temporal resolution whereas the data from the PIV had a high spatial resolution. In total, data was collected for $6\mathrm{s}$ and $4\mathrm{s}$ for HW and PIV, respectively. Further details can be found in Tutkun et al. (2009).

3 Mathematical modeling

3.1 Proper Orthogonal Decomposition

The theory of POD was introduced in turbulence by Lumley (1967) as a mathematical tool to identify structures in turbulent flows with finite total energy. The stochastic turbulent velocity field is decomposed into deterministic scales of motion by finding the deterministic field that has the maximum projection onto the velocity field. This results in a Fredholm integral equation of the second kind. In this study, classical POD was carried out on the PIV data, which gave the following formulation:

$$\int_D R_{ij}(y, y', z, z')\phi_j^{(n)}(y', z')dy'dz' = \lambda^{(n)}\phi_i^{(n)}(y, z), \tag{3.1}$$

where the kernel of the problem is the two-point cross-correlation tensor

$$R_{ij}(y, y', z, z') = \langle u_i(y, z)u_j(y', z')\rangle. \tag{3.2}$$

The coordinate axes are shown in Figure 2.3. Here,$\langle\cdot\rangle$ represents the ensemble average, $\phi_j(y, z)$ is the eigenfunction, λ is the corresponding eigenvalues, and u_i is a fluctuating velocity component from the PIV data. Due to the high spatial resolution of the domain, and the three components of the fluctuating velocity field, the eigenvalue problem is solved for a two-point cross-correlation tensor of size 68949×68949.

In order to reconstruct the velocity field, the random coefficients, $a^{(n)}$, is needed. They are found by projecting the eigenfunction onto the velocity fluctuations as follows:

$$a^{(n)} = \int_D u_i(y, z)\phi_i^{(n)}(y, z)dydz, \tag{3.3}$$

where the integration is performed in the inhomogeneous wall-normal direction (y) and homogenous spanwise direction (z) using the trapezoidal rule. The fluctuating velocities are obtained as a linear combination of eigenfunctions using the random coefficients obtained by (3.3):

$$u_i(y, z) = \sum_{n=1}^{N} a^{(n)}\phi_i^{(n)}(y, z). \tag{3.4}$$

Using this formulation, the POD modes are sorted in descending order of energy content. Figure

3.1 shows the accumulative percentage of energy carried by the POD modes. It should be noted that the total number of modes is 68949, but essentially all the energy lies within the first 500 modes. A partial reconstruction is also possible by using a limited number of modes. That means

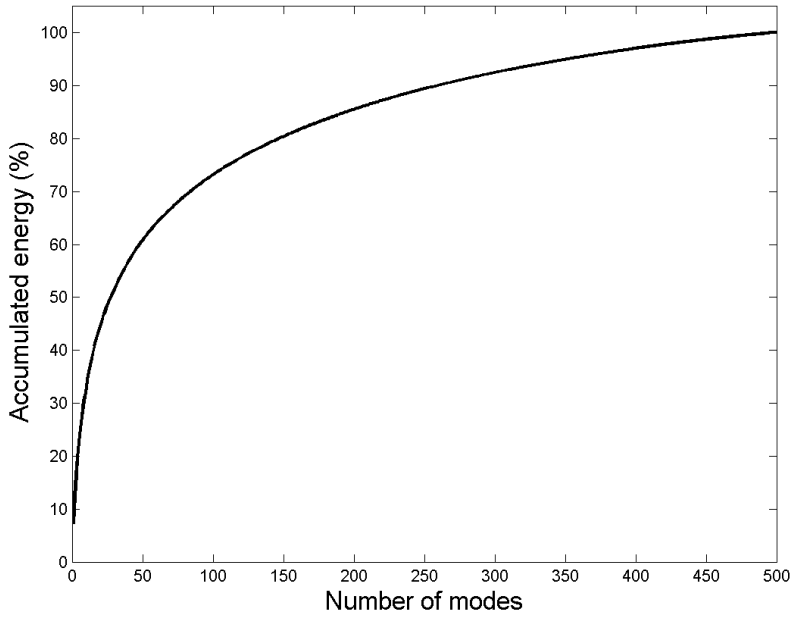

Figure 3.1 Accumulative percentage of energy in the POD modes.

by using the first 28 POD modes the velocity field is reconstructed with only 50% of the energy. Figure 3.2 shows the reconstructed velocity field using 80% and 50% of the total amount of energy. As seen, if the velocity field is reconstructed using less energy, not all of the fluctuations are captured. It should be noted that if the velocity field is reconstructed using all energetic modes, it becomes identical to the original, measured field.

3.2 Linear Stochastic Estimation

In order to obtain a velocity field that is highly resolved in both space and time, linear stochastic estimation (introduced by Adrian (1979)) is used to combine the hot-wire and PIV data. The number of spatial points in the PIV plane is 163×141 whereas the hot wire probes are placed in a 11×13 rake. The PIV measurements are thus more detained in space but the time resolution is much higher at the HW points.

LSE is applied here in order to obtain the temporal resolution of the HW in the PIV plane. The PIV data used can be either the original measured velocity field or the POD reconstructed signal. The method thus correlates the data from the hot-wire measurements to corresponding PIV measurements in order to build two-point correlations that are used to construct a data set with the spatial resolution of the PIV data using only the input from the hot-wire probes. Figure 3.3 shows a schematic picture of this procedure.

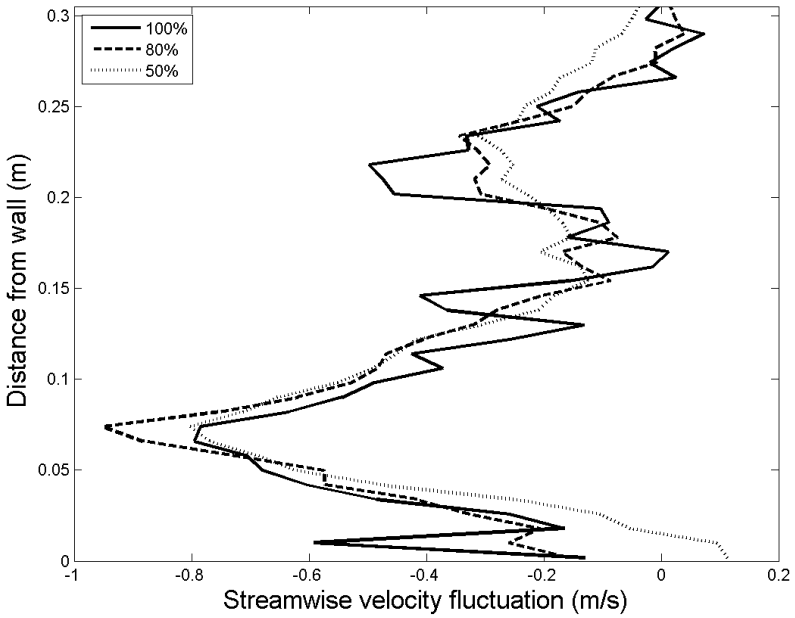

Figure 3.2 Reconstructed instantaneous streamwise velocity fluctuations using different number of modes, i.e., amount of energy. The solid line is the experimental data (equivalent to using 100 % energy), dashed line uses 80 % energy, and dotted line represent 50 % of the energy.

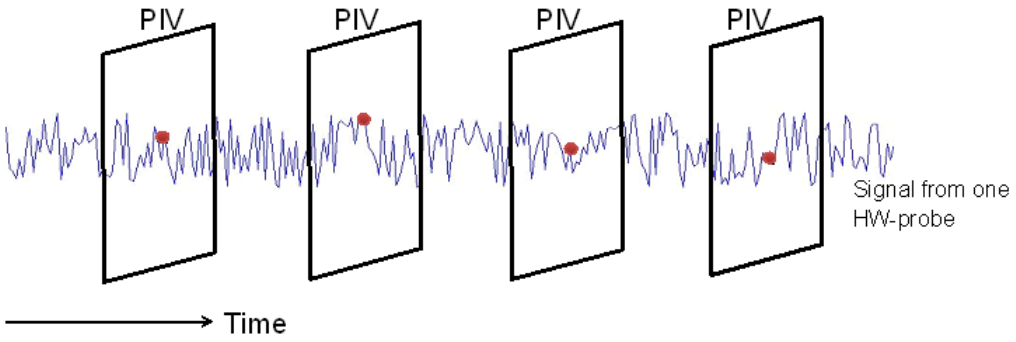

Figure 3.3 Time series of HW and PIV. The blue line shows the velocity signal from one HW-probe. Since the frequency of PIV measurements is much lower than the frequency of the HW, they only coincide at some instances in time, which is shown by the red dots. At these times a two-point correlation coefficient matrix is built, correlating all HW probes with all points in the PIV plane. By only using this coefficient matrix and the signal from the HW, a velocity with the same spatial resolution as the PIV plane and the same temporal resolution as the HW is constructed.

The velocity components at each point p' in the PIV plane is computed as:

$$u_i^{p'}(t) = \sum_{q=1}^{N} A_i^{p'q} u_{HW}^q(t), \tag{3.5}$$

where $N = 143$ is the number of hot-wire probes. Here, primed upper indexes represent points in the PIV-plane whereas regular upper indexes indicate points in the HW-plane (recall that all the measurements are taken in the $y - z$ planes). u_{HW} is the streamwise velocity component given by the hot-wire probes and $A_i^{p'q}$ is the two-point correlation coefficient matrix that is computed according to

$$A_i^{p'q} = \sum_{r=1}^{N=143} \langle u_{HW}^r u_{HW}^q \rangle^{-1} \langle u_{HW}^r u_i^{p'} \rangle. \tag{3.6}$$

The velocity components, $u_i^{p'} = \{u_1^{p'}, u_2^{p'}, u_3^{p'}\}$, used in (3.6) are either the reconstructed velocity field or the original measured PIV data, i.e., not well resolved in time.

Due to the difference in position of the PIV and hot-wire plane the two-point correlations in (3.6) are computed using hot-wire and PIV data at different times. The time difference corresponds to the distance between the measurement planes divided by the convective velocity, i.e., $\Delta t = 0.01/(0.8U_\infty) = 0.00125\text{s}$.

For other examples of the use of linear stochastic estimation and proper orthogonal decomposition see Bonnet et al. (1994)

4 Numerical simulation

The numerical simulations have been performed using the incompressible Navier-Stokes solver Cliff (Cas, 2013). It uses a node based finite volume method, with a fractional-step method for time integration. The simulations are performed using a timestep of $\Delta t = 0.00165s$.

The domain used for the simulations has the form of a rectangular box, with dimensions $L_x \times L_y \times L_z = 3\text{m} \times 0.6\text{m} \times 0.3\text{m}$ in the streamwise (x), wall normal (y) and spanwise (z) direction, respectively. The inlet plane is located at $x = 0$, as indicated in Figure 4.1, and the wall is located at $y = 0$. The top and bottom boundaries ($z = 0\text{m}$ and $z = 0.3\text{m}$, respectively) are considered to be periodic, as indicated in Figure 4.2.

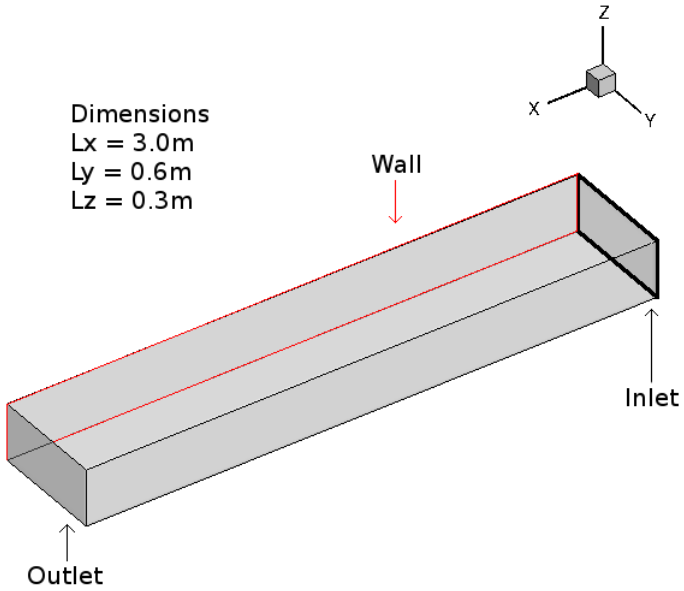

Figure 4.1 *A scetch of the computational domain. L_x is the length in the streamwise direction, L_y is the length in the wall normal direction, and L_z is the length in the spanwise direction.*

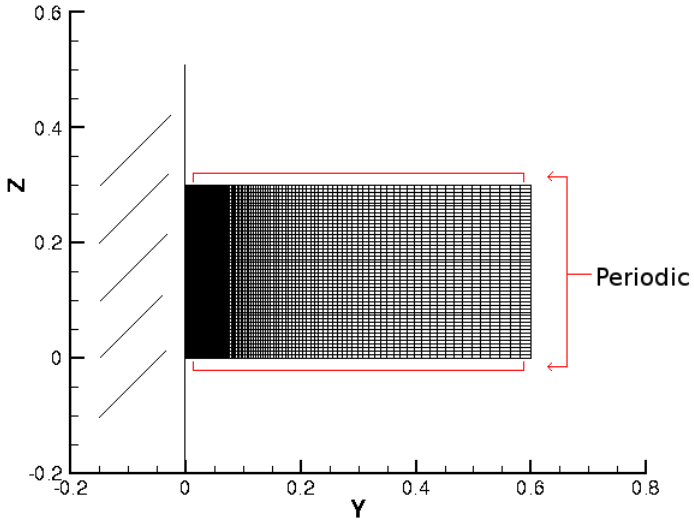

Figure 4.2 *A cross-section of the mesh taken at a constant-X plane. The wall is shown to the left of the mesh at $y = 0$.*

The size of each cell in the mesh is chosen to be dependent on its distance from the wall. A geometric growth is used such that cells close to the wall are much smaller than cells far from the wall (see Fig. 4.2). The distribution of cells in the other directions (x and z) are distributed homogenously. The mesh used contains a total of 15 million cells. The number of cells in each direction is:

$$N_x = 1000, \quad N_y = 150, \quad N_z = 100.$$

4.1 Interpolation of the inflow-data

The inlet profile is generated through the POD-LSE procedure, described in Sections 3.1 and 3.2, on experimental data and fitted to the nodes on the inlet-plane using a linear interpolation. The experimental data exist for the range $y \approx 1\text{mm}$ up to $y \approx 300\text{mm}$. The value for each node is found using inverse distance weighted interpolation.

Since the experimental data is only known for a limited amount of time ($3s$), the inflow data is reused periodically.

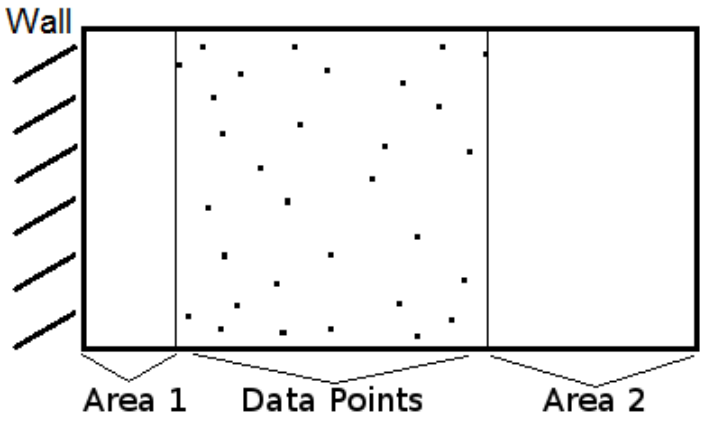

Figure 4.3 Scetch of the different areas in the inlet plane. The different areas are handled separatly in the interpolation. The size of area 1 is greatly exaggregated for easier visualisation (thickness $\approx 2\text{mm}$).

In the area closest to the wall (Area 1 of Figure 4.3), the velocity is set by linear interpolation between the closest available data point and the wall value, which is zero. Nodes in Area 2 of Figure 4.3, are considered to be outside the boundary layer, and the velocity is set to the freestream velocity.

5 Results

Figure 5.1 shows the contours of the instantaneous streamwise velocity gradient at the wall (this quantity is proportional to the frictional force acting on the wall). Elongated structures are clearly visible in the turbulent boundary layer, which is an indication of turbulence streaks. The initial part

(to the left in the figure) shows some effects of the inflow conditions, but after approximately $0.5\mathrm{m}$ this effect seems to have vanished.

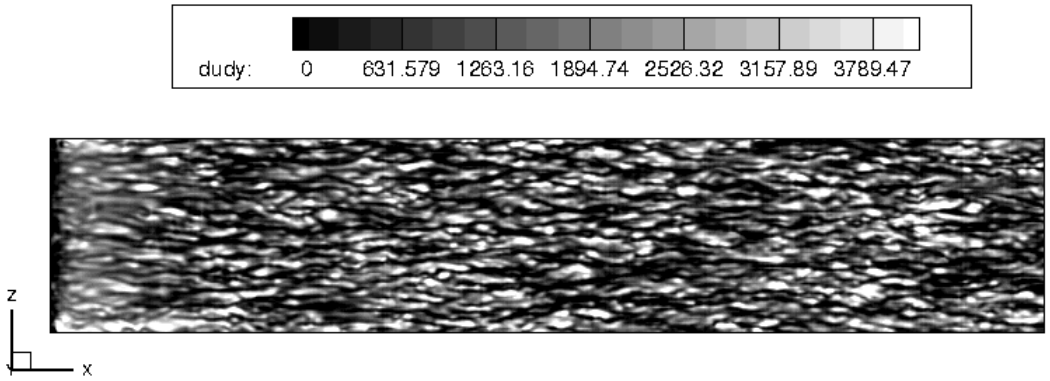

Figure 5.1 Contours of $\frac{\partial u_x}{\partial y}$ at $y = 0$. The flow goes from left to right. Streamwise elongated structures are clearly visible.

Figure 5.2 shows the downstream development of the mean velocity profile, in plus-units, throughout the boundary layer. The theoretical linear and log-layer profiles are also indicated by blue circles and purple line, respectively. The log-law constant has a value much larger than that predicted by theory. This discrepancy is partially explained by an underprediction of the friction velocity due to insufficient spatial resolution. Due to the change of interpolation scheme, the velocity profiles at the inlet has a discontinuous derivative at the transition points (see Figure 4.3). The results show that the discontinuity at the inner transition point is smoothed out already one meter downstream. However, the discontinuity at the outer edge of the boundary layer ($y+ \simeq 3000$) is magnified. Currently, work is in progress to eliminate this artifact.

Figure 5.3 shows the friction velocity, and how it is varying in the streamwise direction, depending on how many POD modes were used in the reconstruction of the velocity field. As seen, there is a significant change in the magnitude of the friction velocity and the length of the transition area depending on the amount of energy. Further downstream, the friction velocity approaches the same value for all energy levels. The transient region for the friction velocity with 100% energy corresponeds well with the length of the region in Figure 5.1 showing effects of the inlet conditions.

Figure 5.4 shows the turbulence kinetic energy profiles at two locations in the domain, the inlet (a) and the outlet (b). The peaks at the inlet stem from the interpolation procedure between Area 1 and the area with the data points in Figure 4.3. In figure 5.4(b) the three non-zero turbulent energy profiles collapse to the same profile at $x = 3.0\mathrm{m}$.

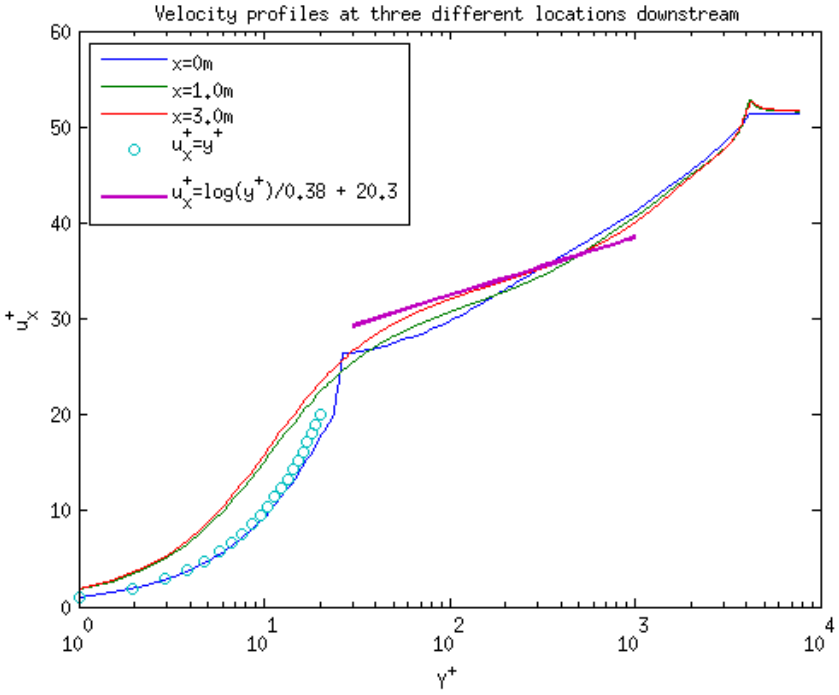

Figure 5.2 Profiles of the $\langle u_x^+ \rangle$ velocity in the wall-normal direction for four downstream locations. The lines $\langle u_x^+ \rangle = y^+$ (law of the wall) and $\langle u_x^+ \rangle = \frac{log(y^+)}{0.41} + 11.5$ (log law) are also shown.

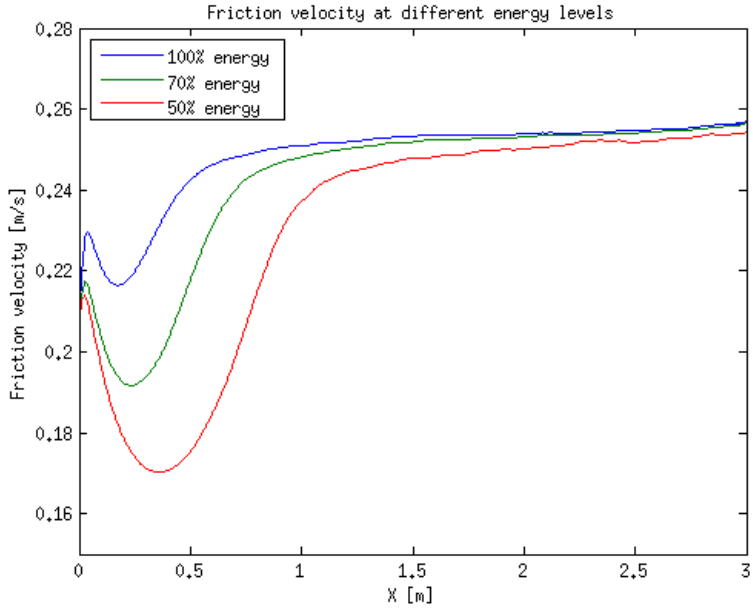

Figure 5.3 Friction velocity over the streamwise domain for different amounts of kinetic energy included in the POD. There is a significant change in the length and magnitude of the transition area.

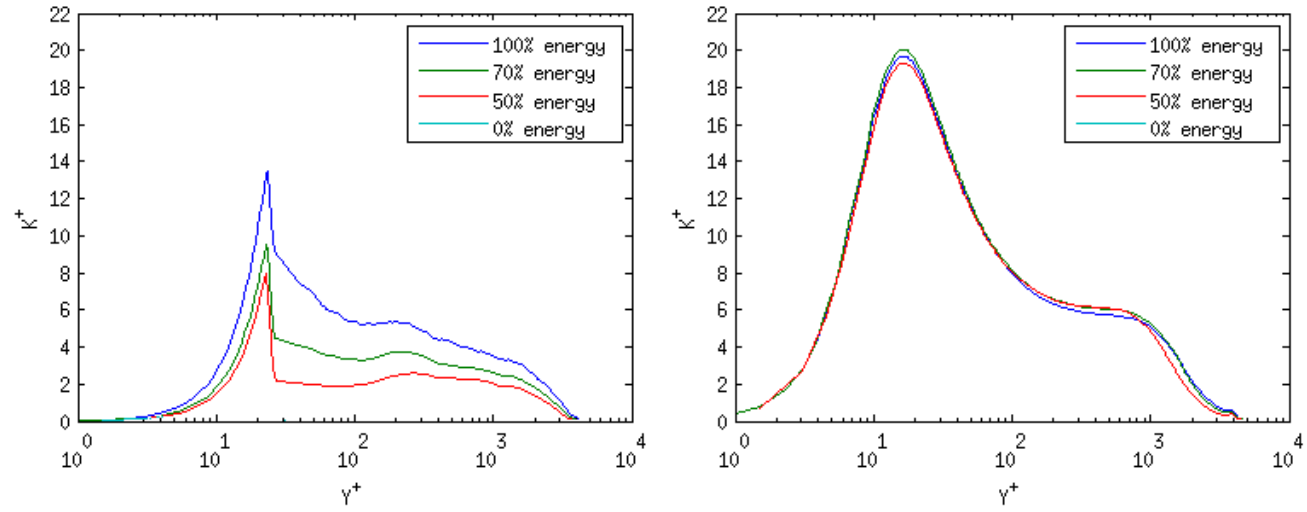

(a) x=0.0m (b) x=3.0m

Figure 5.4 Turbulence kinetic energy at the inlet (a) and outlet (b) of the domain for different number of POD modes. All the profiles, except the one with 0% energy, collapse to the same profile in figure (b).

6 Concluding remarks

In this study, a new method to generate inflow conditions for CFD simulations was investigated. The method utilized an experimental database in order to get realistic velocity fluctuations that are compatible with a solution to the Navier-Stokes equations. By using linear stochastic estimation, the experimental data was expanded to a higher temporal resolution than that given by the original PIV-data. Hence, appropriate inlet conditions with high resolution in both space and time was created.

Numerical simulations using the inlet conditions show promising results; only a small region closest to the inlet seem to be affected by the inflow conditions. This region is considerably smaller than what usually is obtained using other methods. Also, turbulent structures developed in the channel look realistic.

In order to investigate the importance of large scale turbulence on the inlet conditions, proper orthogonal decomposition was used to reconstruct the velocity field with different number of energetic modes. Numerical simulations using 100%, 70%, and 50% were performed and the results showed a longer transition region with less energy captured at the inlet. The turbulence kinetic energy downstream does, however, collapse for all the simulations, indicating that even 50% of the energy is sufficient to capture the large scale dynamics. The present results have a holistically correct shape, but the overall level of turbulence is overpredicted when compared to theory.

References

R. J. Adrian. Conditional eddies in isotropic turbulence. *Physics of Fluids*, 22:2065, 1979.

J. P. Bonnet, D. R. Cole, J. Delville, M. N. Glauser, and L. S. Ukeiley. Stochastic estimation and proper orthogonal decomposition: complementary techniques for identifying structure. *Experiments in fluids*, 17(5):307–314, 1994.

User's & Developer's Manual. Cascade Technologies Inc., 2013.

S. Coudert, J. M. Foucaut, J. Kostas, M. Stanislas, P. Braud, C. Fourment, J. Delville, M. Tutkun, F. Mehdi, P. Johansson, et al. Double large field stereoscopic PIV in a high Reynolds number turbulent boundary layer. *Experiments in Fluids*, 50(1):1–12, 2011.

A. Keating, U. Piomelli, E. Balaras, and H.-J. Kaltenbach. A priori and a posteriori tests of inflow conditions for large-eddy simulation. *Physics of Fluids*, 16:4696, 2004.

J. L. Lumley. The structure of inhomogeneous turbulent flows. *Atmospheric turbulence and radio wave propagation*, pages 166–178, 1967.

T. S. Lund, X. Wu, and K. D. Squires. Generation of turbulent inflow data for spatially-developing boundary layer simulations. *Journal of Computational Physics*, 140(2):233–258, 1998.

P. Moin and K. Mahesh. Direct numerical simulation: a tool in turbulence research. *Annual Review of Fluid Mechanics*, 30(1):539–578, 1998.

M. Tutkun, W. K. George, J. Delville, M. Stanislas, P. B. V. Johansson, J. M. Foucaut, and S. Coudert. Two-point correlations in high Reynolds number flat plate turbulent boundary layers. *Journal of Turbulence*, (10), 2009.